Revised post referee comments (13th Jan '05) **BZ8955**

Surface excitonic emission and quenching effects in ZnO

nanowire/nanowall systems: limiting effects on device potential

J. Grabowska, A. Meaney, K.K. Nanda, J.-P. Mosnier, M.O. Henry, J.-R. Duclère , E. McGlynn*

School of Physical Sciences / National Centre for Plasma Science & Technology,

Dublin City University, Glasnevin,

Dublin 9, Ireland.

* Corresponding author -

Email: enda.mcglynn@dcu.ie

Tel.: ++353-1-7005387

Fax: ++353-1-7005384

ABSTRACT

We report ZnO nanowire/nanowall growth using a two-step vapour phase transport method on a-plane sapphire. X-ray diffraction and scanning electron microscopy data establish that the nanostructures are vertically well-aligned with c-axis normal to the substrate, and have a very low rocking curve width. Photoluminescence data at low temperatures demonstrate the exceptionally high optical quality of these structures, with intense emission and narrow bound exciton linewidths. We observe a high energy excitonic emission at low temperatures close to the band-edge which we assign to the surface exciton in ZnO at ~ 3.366 eV, the first time this feature has been reported in ZnO nanorod systems. This assignment is consistent with the large surface to volume ratio of the nanowire systems and indicates that this large ratio has a significant effect on the luminescence even at low temperatures. The band-edge intensity decays rapidly with increasing temperature compared to bulk single crystal material, indicating a strong temperature-activated non-radiative mechanism peculiar to the nanostructures. No evidence is seen of the free exciton emission due to exciton delocalisation in the nanostructures with increased temperature, unlike the behaviour in bulk material. The use of such nanostructures in room temperature optoelectronic devices appears to be dependent on the control or elimination of such surface effects.

I. INTRODUCTION

ZnO is receiving renewed attention for wide band-gap device applications due to a number of advantages it offers compared with GaN, e.g. larger exciton binding energy, availability of large area substrates for homo-epitaxy etc. [1]. ZnO is a wide bandgap semiconductor (~ 3.37 eV at room temperature), which is suitable for short-wavelength optoelectronic applications. The high exciton binding energy of 60 meV (larger than the thermal energy at room temperature) promises an efficient excitonic emission at room temperature under low excitation intensity [2]. Hence, ZnO is a promising photonic material for UV / blue devices such as short wavelength light emitting diodes and laser diodes in optoelectronics, but also is a promising material for spintronics applications, if doped with magnetic impurities. One–dimensional (1-D) nanoscale materials, such as nanotubes [3], nanowires [4], and nanobelts [5] and other structures [6, 7], have attracted much attention because of their interesting properties and potential to allow exploration of fundamental physical concepts and technological applications [6, 7].

In this paper, we study the low temperature luminescence properties of ZnO nanowire/nanowall systems grown on *a*-plane sapphire, in particular their excitonic properties and the influence thereon of the large surface to volume ratio of these nanostructures. The potential of ZnO nanostructures for next generation device structures is obviously limited by the performance of the material at room temperature. Other authors have commented on various aspects of the impact of large surface to volume ratio on the optical properties of ZnO nanostructures [8, 9]. While the structures that we grow

have been presented in the literature before[10, 11], we present for the first time a detailed study of the effects of the surface to volume ratio on the photonic properties of the nanostructures in the intermediate (50-100 nm) size range and show how critical the surface to volume ratio is in determining the room temperature optical properties and consequently the device potential of the structures.

II. EXPERIMENT

ZnO nanostructures in our experiments are grown on *a*-plane sapphire using vapour phase transport (VPT) via the vapour-liquid-solid (VLS) mechanism using a gold catalyst [4, 10]. In our process, Au (in thin film form) was first deposited on *a*-plane $(11\bar{2}0)$ sapphire substrates. ZnO powder was vaporized and condensed on the substrate via the VLS mechanism (using a two step process). The VLS growth occurs preferentially at grain boundaries in the Au layer resulting in catalysed epitaxial growth of a ZnO nanowall system with a "foam-like" structure, from which nanorods subsequently grow. This mechanism has been described previously by a number of authors [11-13]. The samples are cleaned before any treatments. Gold films of thickness ~ 2 nm are deposited on the substrates prior to growth using a standard bell jar evaporator. These are then annealed at 800°C for 4 minutes leading to growth of grains in the Au layer and a network of grain boundaries. High purity ZnO (99.9995%, Alfa Aesar) powders and high purity C (99.9999%, Alfa Aesar) powders are mixed well at a weight ratio of 1:1. A quartz boat containing both the powder mixture and the substrate is placed in the central hot zone inside a horizontal quartz tube furnace. The two step growth involves preheating the

system to a nominal furnace temperature of 760^0C and cooling to 350^0C. The system is then heated to a nominal furnace temperature of 1125°C and growth takes place for 60 minutes. The system is then cooled to room temperature. This sequence appears to produce extremely high quality material compared to the common one step method in our studies. A high purity (99.999%) 90 sccm Ar flow passes through the quartz tube during the whole process. Comparison with single crystal bulk material was made primarily using a sample obtained from the Eagle-Picher Corporation (EP; USA), and comparison was also made with bulk samples from Rubicon Technology Corporation (RT; USA) and Cermet Inc. (CI; USA).

Samples were characterized by SEM, using a LEO Stereoscan 440 system; XRD, using a Bruker AXS D8 advance texture diffractometer; and PL studies. The PL data were taken using the 325nm line of a continuous wave HeCd laser (output ~ 22mW unfocussed on the sample). The emission from the sample was analyzed using a one metre grating spectrometer (SPEX 1704) and detected with a photomultiplier tube (Hamamatsu model R3310-02) in photon counting mode. Controllable temperatures down to 5 K were achieved using a closed cycle cryostat (Janis SHI-950-5). The typical resolution of the PL data taken in the near band edge region was slightly less than 100 μeV and the absolute energy positions referenced to a calibration source were accurate to ~ 200 μeV. All these data were corrected for the effects of the refractive index of air as appropriate.

III. RESULTS AND DISCUSSION

Figure 1 shows a scanning electron micrograph (SEM) of a sample in the deposited gold region. The figure shows a system of vertically well-aligned nanorods, with evidence of a "foam-like" network of nanowalls below the nanorods. The structure observed is entirely consistent with the reports of Ng *et al* and Lao *et al* [11, 13], who observe a similar nanowall network below a well aligned field of nanorods, as discussed below. The nanorod lengths are quite uniform with a value of ~ 1 μm, and the diameters are slightly less than 100 nm. Nanowall thicknesses are also of the order of 100 nm and the wall heights ~ 500 nm. Vertical growth of the nanostructures is observed, and absence of growth in the region with no gold coverage establishes the VLS mechanism of growth.

Figure 2(a) shows $\theta-2\theta$ x-ray diffraction (XRD) data from this sample, with the ZnO (0002) and (0004) peaks clearly seen at 34.42^0 and 72.56^0 respectively. The absence of any other peaks confirms the good alignment of these nanostructures with *c*-axis along the nanorod axis and perpendicular to the substrate. The 2θ value of the (0002) reflection corresponds to a c-axis lattice parameter of 0.5206 nm, equal (within the instrumental accuracy) to the bulk value of 0.5206 nm [14], as reported by other workers for nanowire growth on this substrate [15]. The rocking curve width of the (0002) peak shown in the inset of figure 2(a) is ~ 0.16^0, one of the lowest values reported to date [15 - 17]. The in-plane ordering of the ZnO nanorods was checked using x-ray phi-scans. Figure 2(b) displays the corresponding phi-scans for the sapphire ($10\overline{1}4$) and ZnO ($10\overline{1}1$) reflections, respectively. It shows six peaks separated by 60^0 and proves that the nanorods are grown

epitaxially on the sapphire with six fold symmetry. The epitaxial relationships between the nanorods and the substrate are $(0001)_{ZnO}$ // $(11\bar{2}0)_{Sapphire}$ and $[11\bar{2}0]_{ZnO}$ // $[0001]_{Sapphire}$, in agreement with other workers [15].

Figure 3(a) shows photoluminescence (PL) spectra of the nanowire/nanowall system taken at both room and low temperatures. The inset in figure 3(a) shows a room temperature PL spectrum of EP single crystal bulk material for comparison. At room temperature (300K), we observe extremely weak band edge luminescence and weak green band emission from the nanostructured sample compared to bulk material, which is often considered as a signature of poor quality material. At low temperatures (figure 3(b)), however, we observe a very strong and sharp band edge emission (measurements at 7 K), with linewidths of ~ 0.6 meV, comparable to good quality bulk material and among the smallest linewidths reported for ZnO nanostructures [15-18]. We also observe the classic "structured" green band, with distinct multi-phonon emission, which is attributed most commonly to either native defects such as oxygen vacancies or Cu-related defects [19, 20]. Thus, the PL data at low temperatures indicate that these samples are of good optical quality. In figure 3(c), we show the near bandedge PL signal of this same sample at 7.75 K as a function of photon energy and also the signal from a EP bulk single crystal sample at 8K. These PL data show a dramatic difference between the room and lower temperature behaviour for the nanorod/nanowall sample. The PL spectra at low temperature for the nanostructured sample are comparable to the bulk material, while the nanostructure emission is strongly quenched at room temperature.

Our low temperature PL data on the nanostructured sample displays five clear peaks at energies of 3.3557(1) eV, 3.3588(1) eV, 3.3598(1) eV, 3.3665(1) eV and 3.3709(1) eV. A range of sharp peaks have previously been observed by a number of authors in studies on single crystal ZnO samples, and have been labelled I_0 to I_{11} [21], though the exact labelling is itself the subject of some controversy, and the microscopic chemical origins of many of the peaks is unknown. The three lower energy peaks at 3.3557(1) eV, 3.3588(1) eV and 3.3598(1) eV may be assigned to the I_9 , I_8 and $I_{6/6a}$ lines associated with bound exciton recombination at neutral donor sites, based on their mutual separations and also their relationship to the well-identified lines [21], we observe in EP bulk material (the lines in the nanostructured material lie a constant 0.8 meV lower than the bulk material). The feature at 3.3709(1) eV is assigned to the I_1 feature based on its localization energy [21] and again is 0.8 meV lower than the corresponding bulk feature. The 0.8 meV shift between the nanostructured sample and the bulk single crystal values most probably indicates either a perturbation due to electric field effects (e.g. due to charge trapping and depletion layers at surfaces[22]) or a small, homogenous strain in the nanostructures. We feel that electric field effects, which are known to lead to substantial broadening, are not consistent with the narrow linewidths we observe in the nanostructured materials [23, 24]. Consequently we conclude that a small, homogenous strain in the sample (below the limits detectable by our XRD instrumentation) is responsible for the lineshifts observed. The fact that we can clearly resolve and identify these lines is an indication of the good optical quality of these nanostructures. The most distinctive feature of this spectrum is the presence of the higher energy line at 3.3665(1) eV, This feature is most likely the I_2 line [21] based on its position, taking into account the strain-induced shift. The feature has not been clearly identified in

ZnO nanorod systems before to the best of our knowledge. The chemical origin of this line is not clear, but the fact that it occurs at such high energy indicates that it may not be due to a "normal" donor bound exciton recombination, and in fact it is associated with an ionized donor bound exciton by some authors [21]. Low temperature studies from the early 1990s [25, 26], however, have identified a high energy line at ~ 368.2 nm (3.3674(1) eV) as due to recombination of a surface-related exciton in ZnO, observed in luminescence studies of a range samples incorporating ZnO crystallites with a high surface to volume ratio. Our results favour this assignment, as the surface to volume ratio of the nanostructures is large and this feature is not observed in the EP bulk crystal material. Figure 4 shows a further comparison between low temperature PL spectra from bulk crystal material from two other suppliers (CI and RT) and EP bulk crystal material. We see no evidence for the surface-related exciton at 3.3665(1) eV in either of these two bulk crystal samples either, although both show significant luminescence from various members of the I-line series[21].

Figure 5(a) shows the evolution of the PL spectra for the nanowall/nanorod sample as a function of temperature in the band-edge region. We note that the surface exciton at ~ 3.366 eV vanishes faster than the other lower energy bound exciton features and is gone at 20K, while the luminescence from the other features survives to ~ 70K and all these features appear to vanish at approximately the same rate. No other lines appear in a broader spectral range (3.300-3.440 eV) with increasing temperature. Figure 5(b) shows equivalent data for the EP bulk single crystal sample, where the bound exciton signals survive up to ~ 130K. In figure 5(c), we show the fits of the intensity versus temperature

data to a temperature-activated exciton dissociation process for (i) the integrated emission of the I_9 , I_8 and $I_{6/6a}$ lines in the nanostructured sample, (ii) the surface exciton feature in the nanostructured sample and (iii) the integrated intensity of the I_9 , I_8 , $I_{6/6a}$ and I_4 lines in the EP bulk single crystal sample. These fit well with activation energies ΔE of 6.5 ± 0.8 meV, 5 ± 1.5 meV and 13 ± 0.6 meV, respectively. The value for the EP bulk sample is reasonably close to the average bound exciton localization energy for these features ~ 16 meV [21], and indicates a normal thermally induced exciton dissociation. However, the activation energies for the nanostructured sample are very significantly lower than any of the exciton localisation energies, indicating a substantially different process is occurring. This is further evidenced by the growth for the bulk sample of free exciton emission which becomes prominent for temperatures above ~ 50K (figure 5(b) and the absence of any free exciton luminescence in the nanostructured sample with increasing temperature.

We propose that the large surface to volume ratio which gives rise to the appearance of surface excitonic features at low temperatures is also responsible for the rapid decay of the luminescence with increasing temperature via a temperature-activated non-radiative recombination process for excitons at surface states. This explains both the rapid decay of the bound exciton features and the absence of any free exciton luminescence in the nanostructured sample. This process may occur, for example, via ionisation of surface states responsible for the surface excitonic PL at low temperatures, to create non-radiative surface traps. One may clearly demonstrate the effect of this nonradiative recombination by studying the behaviour of the full width at half maximum height (FWHM) of the I_9 peak (which can be observed in both samples) as a function of

temperature. This is shown in figure 6(a). We observe that linear fits to these data give value of ~ 4 μeV/K for the EP bulk crystal and ~ 12 μeV/K for the nanostructured sample. The value for the bulk material compares well with previous measurements of thin film material [27], but the FWHM in the nanostructured sample increases at a much higher rate, indicating either a drastic change in the nature of the exciton-phonon scattering processes or the presence of additional quenching mechanisms shortening the exciton lifetime, which we propose to be surface-related. In the temperature region 10-70K, exciton-acoustic phonon scattering processs typically dominate the increase of FWHM leading to a linear behaviour [28]. We examine the exciton-phonon processes in the nanostructures by studying the variation of the exciton energies as a function of temperature, which are again dominated by similar electron-phonon interactions in this temperature range, shown in figures 6(b) and (c) for the nanostructured and EP bulk samples, respectively. A Varshni fit [29] (shown in figures 6(b) and (c)) to the various bound exciton lines observed in both samples yields values for the α and β Varshni parameters, respectively. The average values of these parameters for the bulk sample are $\alpha_{bulk} = 0.49$ meV/K $\pm$ 0.1 meV/K and $\beta_{bulk} = 1000K \pm 200K$. For the nanostructured sample the values are $\alpha_{nano} = 0.48$ meV/K $\pm$ 0.1 meV/K & $\beta_{nano} = 900K \pm 200K$. These are in good agreement with literature values [21, 30] and certainly do not indicate any major change in the nature of the electron-phonon interactions (which determine α and β) for the two systems. We note that the Varshni fit for the bulk crystal sample is chosen to best fit the data below 70K, for comparison with the nanostructured material. The three parameter Varshni fit is known not to fit such data sets accurately over a wide temperature range [31], but over the 10 - 70K range the fit qualities are comparable and the

fit parameters, particularly the β factor, indicate the strength of the electron-phonon coupling. We conclude that the effects we observe are caused by the large nanostructure surface to volume ratio, and note that such effects have been observed by other authors [8, 9]. We also note that in similar studies of nanorods grown by MOCVD [15] quite different data are reported with nanorod luminescence surviving to high temperature (~150K) and observation of free exciton features at higher temperatures also. Thus, the detail of the growth conditions and passivation mechanisms in various growth methods appear key to the use of the good optical properties of these systems at room temperature and subsequent device development.

IV. CONCLUSION

We have studied the growth of ZnO nanowall/nanorod systems on *a*-plane sapphire using a vapour phase transport mechanism. XRD and SEM data indicate that these nanostructures are well-aligned with *c*-axis normal to the substrate, with a very low rocking curve halfwidth. PL data show that the optical quality of the nanowires is excellent at low temperatures, with intense emission and narrow bound exciton linewidths. Temperature dependence measurements of the PL show a temperature-activated non-radiative mechanism limiting the utility of these structures for room temperature devices. We observe a high energy excitonic emission close to the band edge which we assign to the surface exciton in ZnO at ~ 3.3665(1) eV, consistent with the large surface to volume ratio of the nanostructures. These surface effects are also responsible for the rapid decay of the luminescence with increasing temperature. These

observations all lead us to conclude that in the systems we have grown, the large surface to volume ratio detrimentally affects the optical properties of the system, and the excellent low temperature optical properties are not apparent at room temperature. These nanostructures offer the prospect of extremely efficient excitonic emission for device applications, but the control of surface effects via passivation or other means will be an important task in order to realise devices at room temperature.

ACKNOWLEDGEMENTS

REFERENCES

[1] D.C. Look, Mat. Sci. & Eng. B **80**, 383 (2001).

[2] M. H. Huang, S. Mao, H. Feick, H. Yan, Y. Wu, H. Kind, E. Weber, R. Russo, P. Yang, Science **292**, 1897 (2001).

[3] Y. J. Xing, Z. H. Xi, Z. Q. Xue, X. D. Zhang, J. H. Song, R. M. Wang, J. Xu, Y. Song, S. L. Zhang, D. P. Yu, Appl. Phys. Lett. **83**, 1689 (2003).

[4] M. H. Huang, Y. Wu, H. Feick, N. Tran, E. Weber, P. Yang, Adv. Mater. **13**, 113 (2001).

[5] X.Y. Kong, Z.L. Wang, Appl. Phys. Lett. **84**, 975 (2004).

[6] W.L. Hughes, Z.L. Wang, J. Am. Chem. Soc.**126**, 6703 (2004).

[7] Z.L. Wang, X.Y. Kong , J.M. Zuo, Phys. Rev. Lett. **91**, article 185502 (2003).

[8] I. Shalish, H. Temkin, V. Narayanamurti, Phys. Rev. B **69**, article 245401 (2004).

[9] S. Hong, T. Joo, W.I. Park, Y.H. Jun, G.C. Yi, Appl. Phys. Lett. **83**, 4157 (2003).

[10] J.T. Hu, T.W. Odom, C.M. Lieber, Acc. Chem. Res. **32**, 435 (1999).

[11] H.T. Ng, J. Li, M.K. Smith, P. Nguyen, A. Cassell, J. Han, M. Meyyappan, Science **300**, 1249 (2003).

[12] B. Nikoobakht, A. Davydov, S.J. Stranick, Mat. Res. Soc. Symp. Proc. **818**, M8.25.1-6 (2004).

[13] J.Y. Lao, J.Y. Huang, D.Z. Wang, Z.F. Ren, D. Steeves, B. Kimball, W. Porter, Appl. Phys. A **78**, 539 (2004).

[14] *Landolt-Bornstein, Numerical Data and Functional Relationships in Science and Technology – New Series III, Vol. 41B*, edited by U. Rossler (Springer, Berlin 1999)

[15] B.P. Zhang, N.T. Binh, Y. Segawa, Y. Kashiwaba, K. Haga, Appl. Phys. Lett. **84**, 586 (2004).

[16] B.P. Zhang, N.T. Binh, Y. Segawa, K. Wakatsuki, N. Usami, Appl. Phys. Lett. **83**, 1635 (2003).

[17] W.I. Park, D.H. Kim, S.-W. Jung, G.C. Yi, Appl. Phys. Lett. **80**, 4232 (2002).

[18] M. Lorenz, J. Lenzner, E.M. Kaidashev, H. Hochmuth, M. Grundmann, Ann. Phys. (Leipzig) **13**, 39 (2004).

[19] R. Dingle, Phys. Rev. Lett. **23**, 579 (1969).

[20] K. Vanheusden, W.L. Warren, C.H. Seager, D.R. Tallant, J.A. Voight, B.E. Gnade, J. Appl. Phys. **79**, 7983 (1996).

[21] B.K. Meyer, H. Alves, D.M. Hofmann, W. Kriegseis, D. Forster, F. Bertram, J. Christen, A. Hoffmann, M. Strassburg, M. Dworzak, U. Haboeck, A.V. Rodina, Phys. Stat. Solidi (b) **241**, 231 (2004).

[22] C. Roy, S. Byrne, E. McGlynn, J-P Mosnier, E. de Posada, D. O'Mahony, J. G. Lunney, M. Henry, B. Ryan, A.A. Cafolla, Thin Solid Films, **436**, 273 (2003).

[23] E. McGlynn, J. Fryar, G. Tobin, C. Roy, M. O. Henry, J. -P. Mosnier, E. de Posada, J. G. Lunney, Thin Solid Films **458**, 330 (2004).

[24] D.F. Blossey, Phys. Rev. B **3**, 1382 (1971).

[25] V.V. Travnikov, A. Freiberg, S.F. Savikhin, J. Lumin. **47**, 107 (1990).

[26] S.F. Savikhin, A. Freiberg, J. Lumin. **55**, 1 (1993).

[27] X.T. Zhang, Y.C. Liu, Z.Z. Zhi, J.Y. Zhang, Y.M. Liu, D.Z. Shen, W. Xu, G.Z. Zong, X.W. Fan, X.G. Kong, J. Phys. D: Appl. Phys. **34**, 3430 (2001).

[28] R. Hellmann, M. Koch, J. Feldmann, S.T. Cundiff, E.O. Gobel, D.R. Yakovlev, A. Waag, G. Landwehr, Phys. Rev. B **48**, R2847 (1993).

[29] Y.P. Varshni, Physica **34**, 149 (1967).

[30] S. Ozaki, T. Mishima, S. Adachi, Jpn. J. Appl. Phys. **42**, 5465 (2003).

[31] R. Passler, Phys. Stat. Solidi (b) **200**, 155 (1997).

FIGURE LEGENDS

Figure 1: Two SEM images of a ZnO nanorod/nanowall sample grown on a-plane Al_2O_3.

Figure 2: (a) $\theta-2\theta$ XRD data of the sample in figure 1. ZnO (0002) and (0004) peaks are at 34.42^0 and 72.56^0 respectively. Sapphire $(11\bar{2}0)$ peak is seen at ~ 37.78^0. Inset shows the rocking curve of this sample, with a width of ~ 0.16^0. (b) Phi-scans of the sapphire $(10\bar{1}4)$ / ZnO $(10\bar{1}1)$ planes for this sample.

Figure 3: PL data at room temperature (a) and 7 K (b) for the nanostructured sample. The y-axis range of 3(b) is one hundred times that of 3(a). Figure 3(c) shows PL data and line identifications at low temperatures for the nanostructured sample in comparison with an Eagle-Picher (EP) single crystal bulk sample. The inset in 3(a) shows a room temperature PL spectrum of EP single crystal bulk material.

Figure 4: Comparison of low temperature PL (at 7.5K) from two other sources of bulk single crystal ZnO; Rubicon Technologies (RT) and Cermet Inc. (CI), in addition to the EP sample.

Figure 5: Evolution of PL spectra as a function of temperature for (a) nanostructured sample and (b) EP bulk crystal. 5(c) shows the fits (solid lines) to a temperature activated process with activation energies displayed.

Figure 6: (a) evolution of FWHM of I_9 line in EP bulk and nanostructured material with temperature. (b) & (c) variation of excitonic energies with temperature for nanostructured and EP bulk samples, respectively. Solid lines are fits to Varshni model discussed in the text.
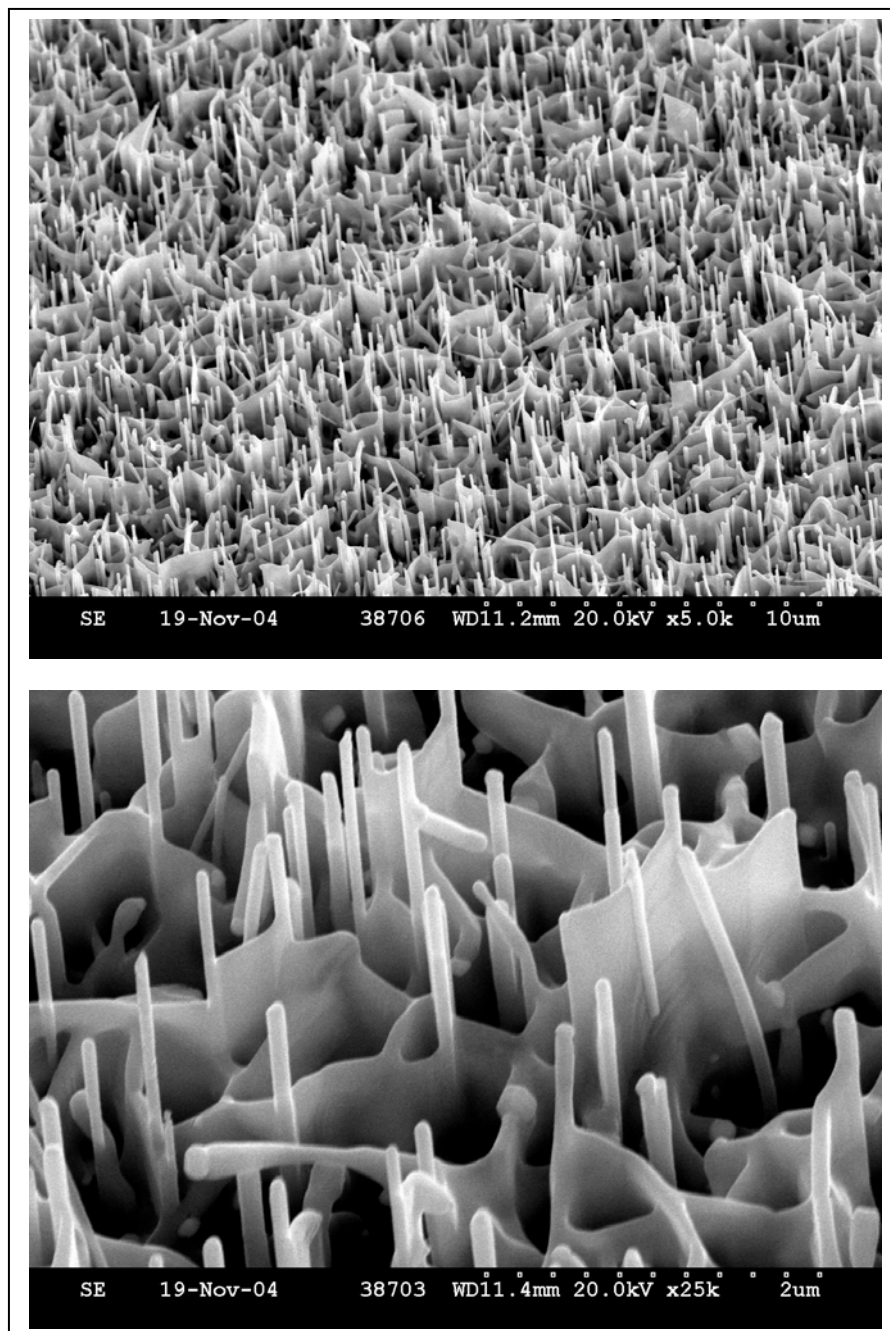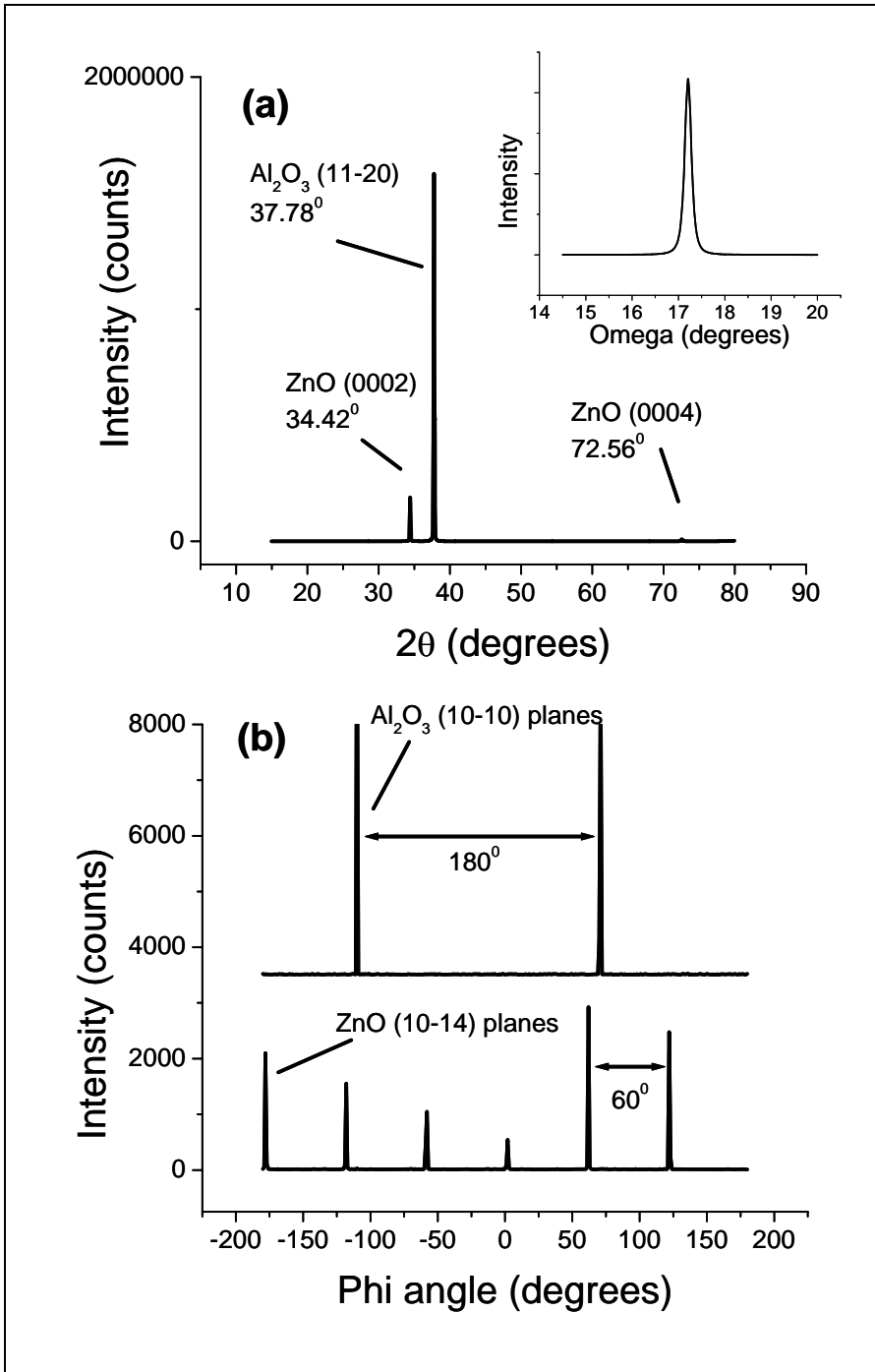
Figure 1

J. Grabowska et al.

"Surface excitonic emission and quenching effects in ZnO nanowire/nanowall systems: limiting effects on device potential"
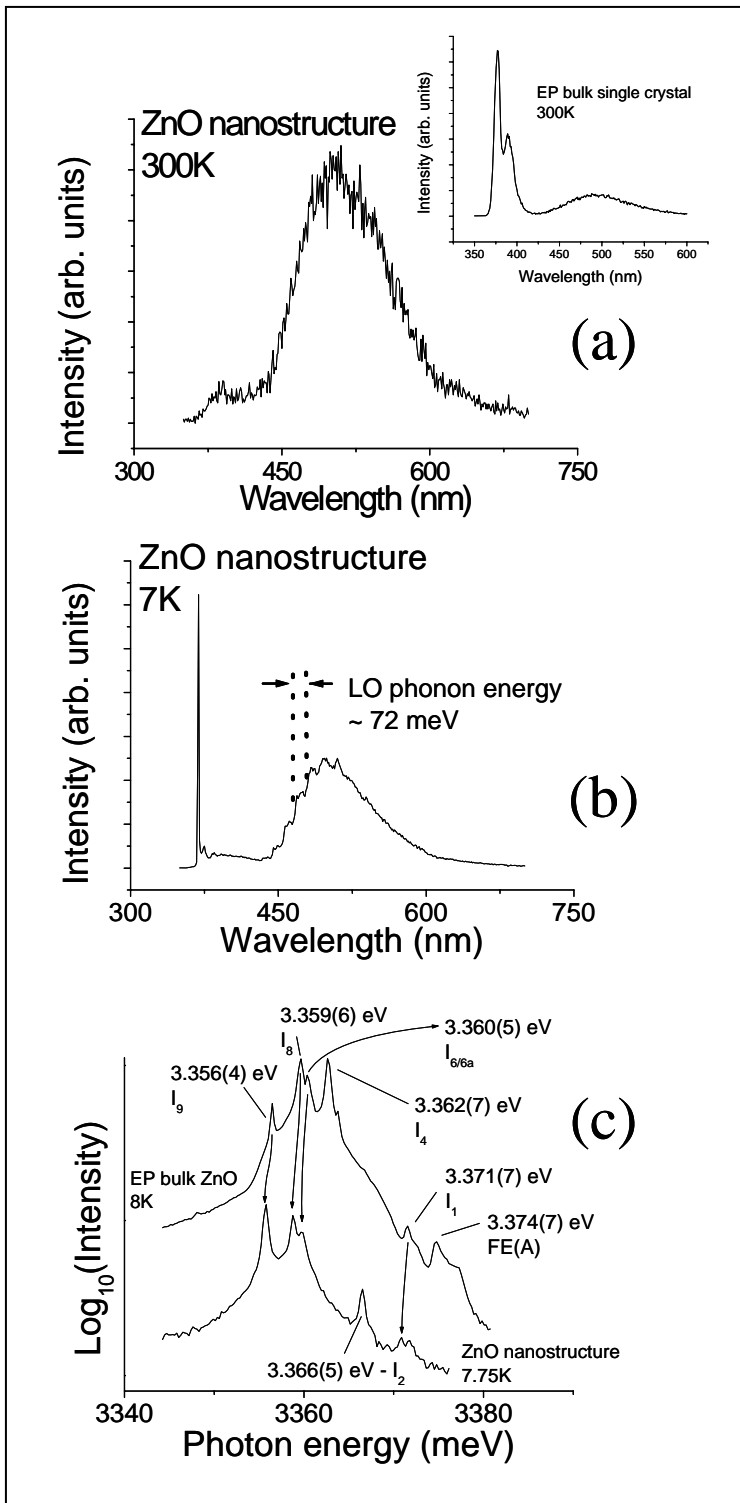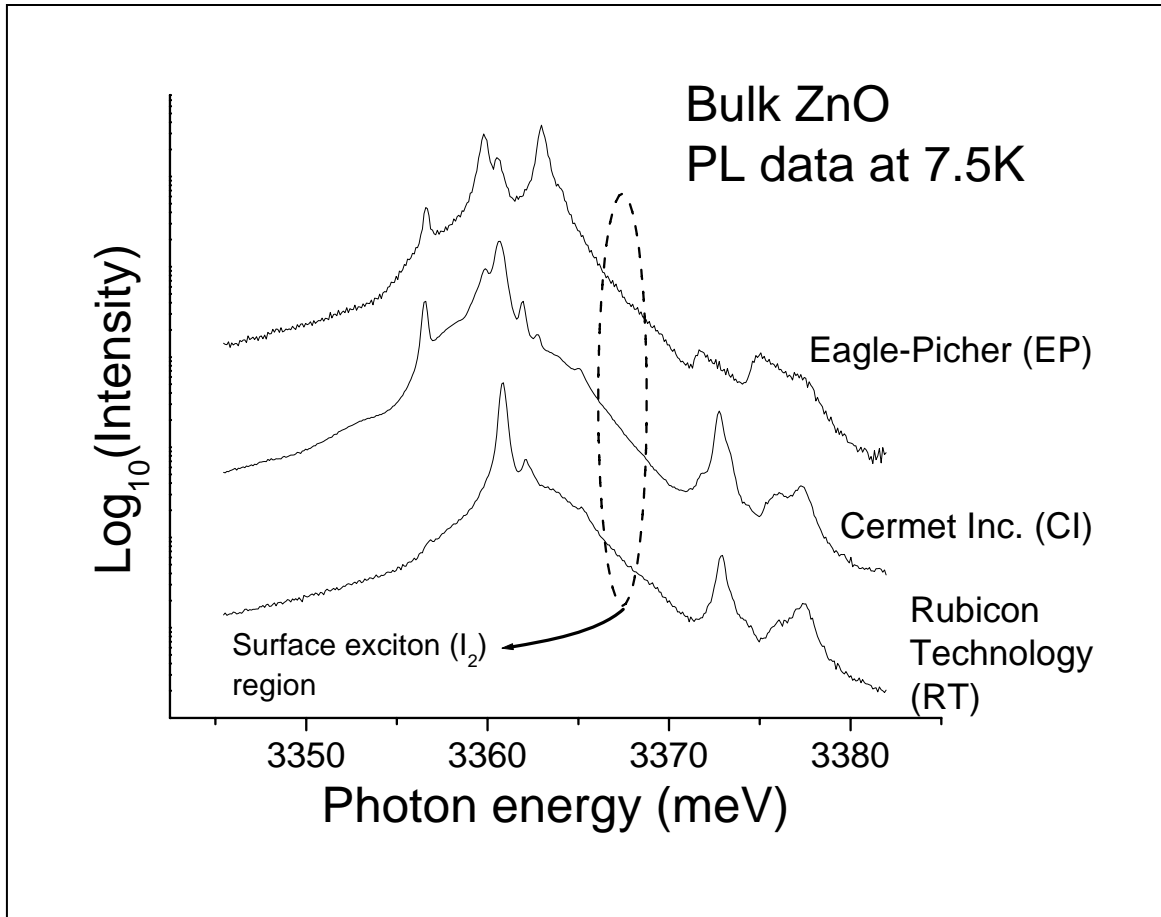
Figure 2

J. Grabowska et al.

"Surface excitonic emission and quenching effects in ZnO nanowire/nanowall

systems: limiting effects on device potential"

Figure 3

J. Grabowska et al.

"Surface excitonic emission and quenching effects in ZnO nanowire/nanowall systems: limiting effects on device potential"
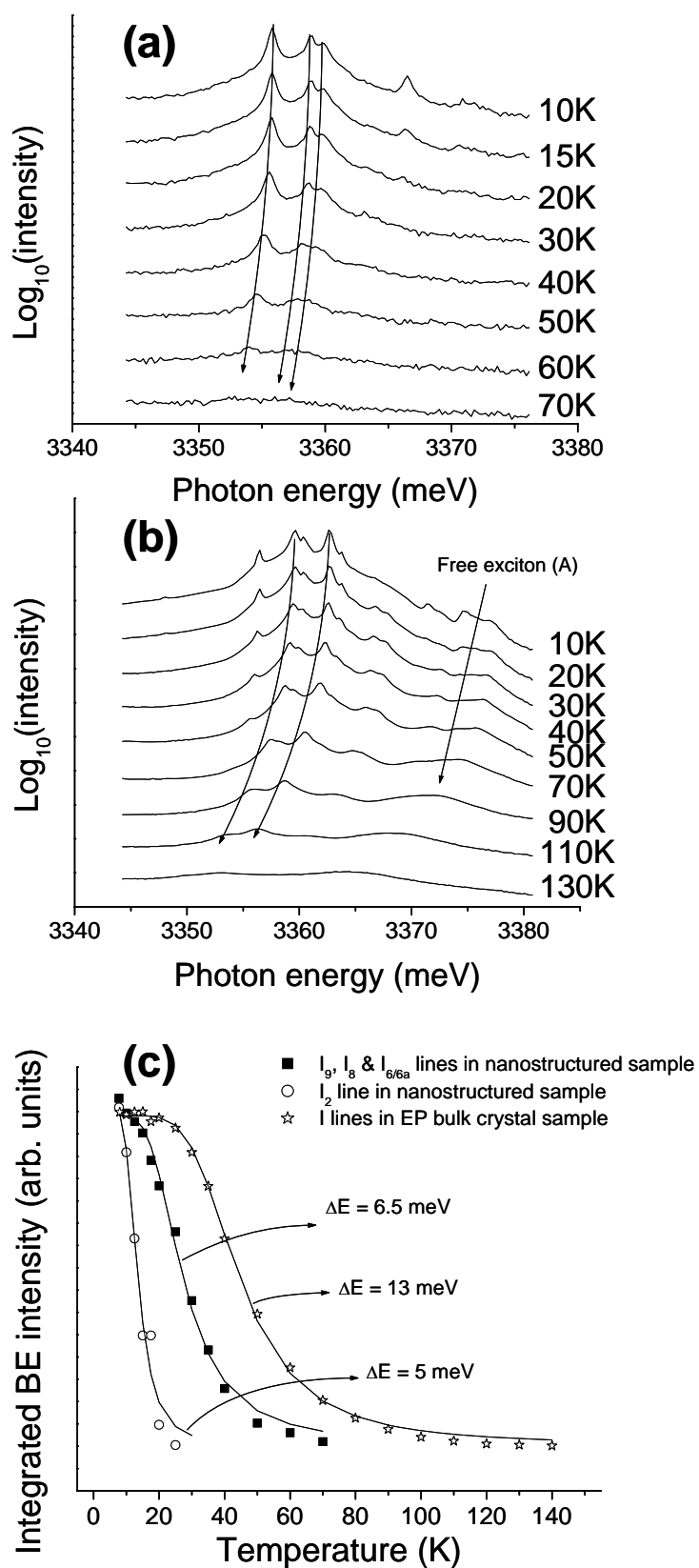
Figure 4

J. Grabowska et al.

"Surface excitonic emission and quenching effects in ZnO nanowire/nanowall

systems: limiting effects on device potential"

Figure 5

J. Grabowska et al.

"Surface excitonic emission and quenching effects in ZnO nanowire/nanowall systems: limiting effects on device potential"
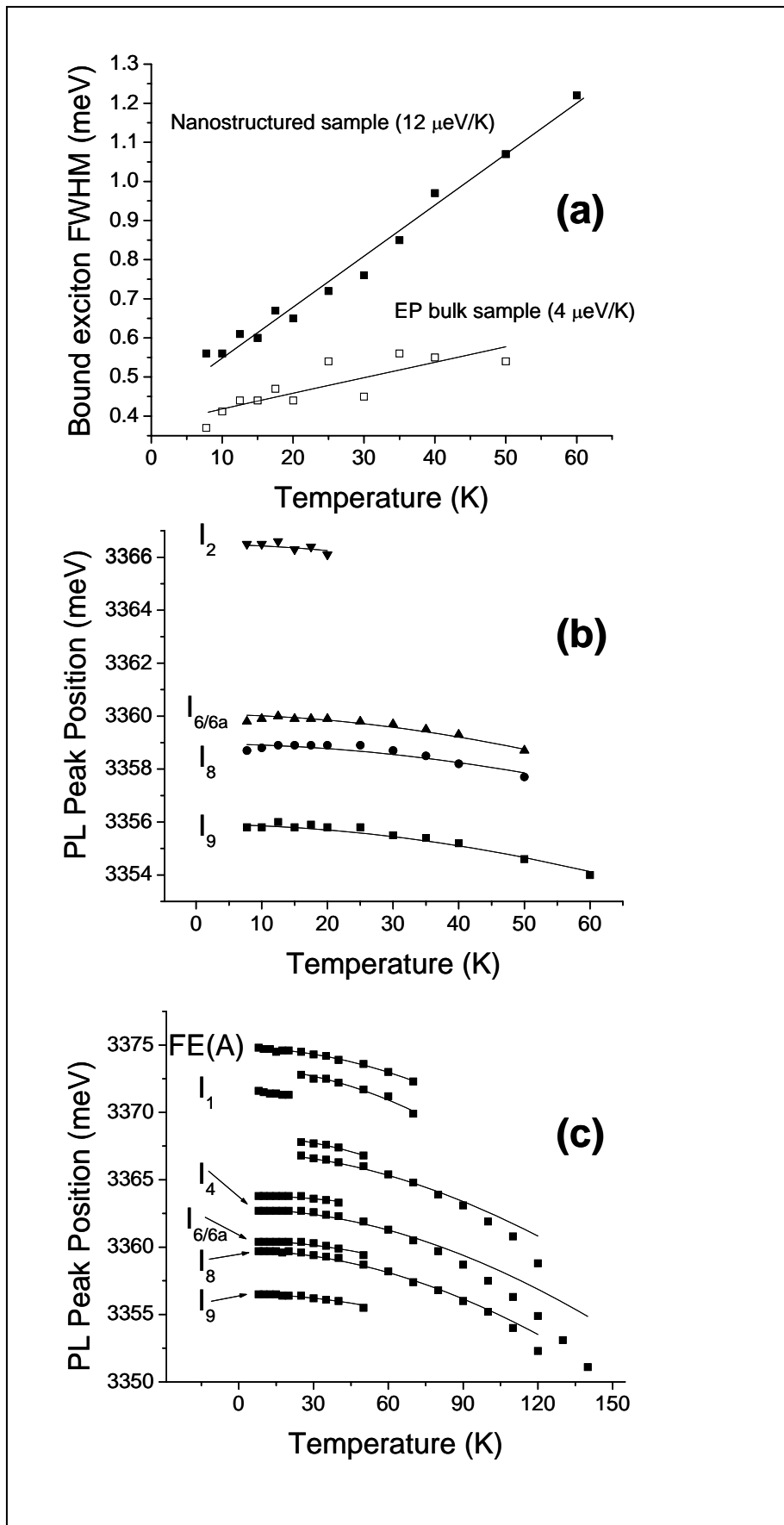
Figure 6

**J. Grabowska et al.
"Surface excitonic
emission and quenching
effects in ZnO
nanowire/nanowall
systems: limiting effects
on device potential"**